 ISSN:2302-8149
e-ISSN:2540-9719

Enhancing the Diagnosis of Cerebral Vascular Occlusion in Brain MRI Images using Advanced Image Processing Techniques

[1]Alhan Anwr Younis AL-Safar*, [2]Intesar Al-Asa'ad
[1]*Department of Arabic Language, College of Education for Women, University of Mosul, Mosul, Iraq*
[2]*Nineveh Education Directorate, Nineveh, Iraq*
*e-mail: alhan.alsafar@uomosul.edu.iq

(***received*:** 18 January 2026, ***revised*:** 8 February 2026, ***accepted*:** 30 March 2026)

Abstract

The paper presents an automated and computationally lightweight system that aims at diagnosing the presence of the ischemic stroke in the brain based on the MRI images and prioritizes mathematical clarity over the overpowering complexity. Workflow starts with AWCES algorithm to improve the quality of images, which is applied based on adaptive windowing determined by the entropy, and then proceeds to Watershed segmentation based on markers to word out the areas that are suspected of being vascularly blocked. The texture descriptors are then obtained using the Local Binary Patterns (LBP) and sent to a Random Forest classifier which differentiates between the damaged and the healthy brain tissue. The training stage has been integrated with the SMOTE technique to address the problem of class imbalance that is severe in the dataset. With a stratified five-fold cross-validation, the system demonstrated an AUC of 0.99, a specificity of 94% and a recall of 70%. These results indicate that the classical methods based on open mathematics can be competitive with deep learning networks, providing a high-quality and quick diagnostic methodology that could be used as a primary solution in the diagnosis of a stroke and as a complement to the exploratory three-dimensional visualization.

Keywords: cerebral vascular occlusion, contrast enhancement, ischemic stroke, magnetic resonance imaging (MRI), medical image processing, random forest classification.

1. Introduction

Digital image processing is currently one of the key foundations of medical imaging that allows improving the quality of images based on mathematically-based processes that are customized to the needs of a specific diagnostic case. Some of these core operations like noise reduction, contrast enhancement, and resolution enhancement bear far-reaching clinical weight [1, 2], and especially when reading magnetic resonance imaging (MRI) data, those operations add value extensively to the clinical ability to detect fine pathological changes and subtle anatomical structures, and thus enable the physician to make sounder decisions at more opportune times.

The cerebrovascular diseases remain on the list of the greatest health issues of modern medicine all over the world [3]. Epidemiological studies dating back as far as 1900 to 2000 have confirmed this fact by placing ischemic stroke on top of the list of the causes of death and chronic disability over the last century or so [3, 4]. The most noticeable pathological etiology of such a stroke is in the blockage of cerebral vessels, that is, the blocking of blood circulation in intracranial arteries, resulting in localized deficits in perfusion and irreversible neurological damage. Not only the blockage of large vessels is a matter, but also small vessel disease, the diagnosis of which is complicated further by the insensibility of the imaging manifestations [4, 5]. This clinical spectrum is also expanded to cover such conditions like subarachnoid hemorrhage [6], which is not any less urgent in its demand of prompt intervention to improve the outcomes [7].

The factor of time is decisive when it comes to treating acute ischemic stroke where numerous scientific studies have shown that the rate at which a therapy is instigated, especially by the use of intravenous thrombolysis or catheter-delivered thrombectomy, has a direct relationship with

 ISSN:2302-8149
e-ISSN:2540-9719

neurological outcome and reduced mortality [8]. Based on this position, well-coordinated fast-response procedures have arisen [9, 10], which subsequently require dynamic, expedited and repeatable diagnostic mechanisms so that advanced reperfusion therapies can be provided within the suitable time period [11, 12].

The magnetic respiratory imaging takes a predominant role in detecting and characterizing cerebrovascular disease. Its images are, however, a technically complex task to read, particularly when it comes to low-contrast lesions or newly formed infarcts, and highly specialized expertise becomes inevitable. Recent works taking advantage of open-source databases have demonstrated potential opportunities of the deep learning systems in helping the radiological reader and reducing the differences between various interpreters [13]. With this advancement, and consideration of the ongoing clinical requirement of readily accessible and computationally efficient diagnosis tools, the current study suggests a coherent and integrated approach to enhancing MRI-based diagnosis of cerebrovascular blockage with special focus on presenting the spatial positioning of the blockage with explicit color coding [14].

The research question in this case is main: can it be possible to create a well-designed classical image processing pipeline without deep neural networks to achieve the same diagnostic performance as the modern options between binary classification of ischemic and healthy brain MRI images of the brain? The main clinical rationale of this question is the slowness of the time-consuming manual interpretation of the image that can be an obstacle to providing speedy treatment. To this end, the main objective of this research is to design and systematically test an automated system whose steps involve adaptive contrast enhancement, morphological cue-based segmentation, minimizing the quantitative texture features, and traditional machine learning-based classification, with the aim of increasing the accuracy as well as the speed of diagnosing cerebral vascular occlusion. The secondary objective is, in its turn, to generate clinically meaningful color-coded two-dimensional overlays and an exploratory three-dimensional visualisation of the affected area, thus contributing to quicker clinical decisions with clearer information.

1.1. Related Work

There has been an increased research attention in the field of automated analysis of brain MRI scanning to detect vascular diseases, and much of the previous literature has focused on investigating each of the system subsystems under different settings and conditions. The models based on global histogram approaches have more or less been giving way to adaptive contrast enhancement techniques which prove to be the more appropriate choice of enhancing local details in medical images. Some researchers have narrowed their attention to varieties of adaptive histogram equalization in order to help bring out obscured pathological effects in MRI images [11], other researchers have tried to use methods of entropy-based contrast scaling in order to increase the output of diagnostic data without overemphasizing noise [12]. In this perspective, the AWCES model proposed in the current study, a hybrid between adaptive window-based contrast stretching and entropy-guided parameter tuning, can be thought of as being similar in spirit to these previous lines of approach.

On the image segmentation side, the region-growing algorithm as well as Watershed transform have received wide acclaim in groups of individuals engaged with medical image processing. With its conceptual transparency, and ability to form spatially connected structures meeting preset homogeneity criteria, the region-growing algorithm has been applied to segment MRI scans of anatomical landmarks and lesion types of various types [14]. Conversely, the Watershed transform demonstrates significant capability in teasing out the borders of complicated and overlaying structures, like the intracranial vascular web by relying on gradient-based topographical data which ensure that edges are precisely positioned [15]. Hybrid segmentation methods which leverage the complementary nature of the two have also been proposed beginning with a region based initialisation, followed by refinement step with Watershed [16], an algorithm that is strongly associated with the definition of vascular occlusion areas with stability and reliability.

 ISSN:2302-8149
e-ISSN:2540-9719

In medical image classification systems, texture analysis takes central place in the feature extraction stage of the system. Gray-Level Co-occurrence Matrix (GLCM) descriptors such as contrast, correlation, energy and homogeneity have demonstrated long-standing performance in the various classifications which assist in identifying healthy versus diseased tissue using various imaging modalities [17]. Parallel, Local Binary Patterns (LBP) have garnered significant interest due to their low computation cost, and their inherent resistance to monotonic gray-level deformations, which has seen them used repeatedly in tissue classification and lesion detection in MRI scans [18]. The individual medical scenarios, where LBP and GLCM have been compared have also demonstrated the discriminatory nature of all these representations [19]. The current methodology has opted to incorporate these two families of features as a personage characteristic of the area that is suspected of vascular occlusion.

With regard to the Random Forest classifier, the company has positioned itself in medical informatics by being in a position to deal with high-dimensional feature spaces, intrinsic resistance to overfitting due to the ensemble voting mechanism, and provision of interpretable rankings of feature importance [20]. As with applications to the detection of brain diseases in MRI, which are usually coupled with texture descriptors, including LBP or GLCM, it has always produced competitive diagnostic results [21]. Such systems have also been evaluated based on indicators like the AUC of the ROC curve, the F1 score and the classification accuracy which are reference metrics of accepted standing [22]. Most of these methodological aspects have already been covered in the literature separately but the combination of these parts in the proposed order, i.e. contrast enhancement using AWCES, then segmentation using region growing or Watershed, then feature extraction using LBP or GLCM, and then classification using Random Forest, to the specific purpose of diagnosing cerebral vascular occlusion with a color visual representation, is a novel and distinct contribution made by this study. A systematic comparative summary of the most well-known reference studies that are near to this orientation is provided in Table 1 [22].

Table 1 Structured comparison of related studies in medical image analysis

Study Ref.	Imaging Modality	Target Application	Contrast Enhancement	Segmentation	Feature Extraction	Classifier	Key Contribution
[11]	MRI	Brain Tumor Visibility	Adaptive Histogram Eq.	Manual	Morphological	SVM	Enhanced tumor delineation
[12]	CT	Abdominal Lesions	Entropy-guided	Semi-automated	Intensity-based	Thresholding	Optimized enhancement parameters
[14]	MRI	Liver Lesion Segmentation	Standard Preprocessing	Region Growing	Statistical	k-NN	Automated lesion volume estimation
[15]	MRA	Cerebral Vasculature	None specific	Watershed + markers	Vesselness filters	N/A	Accurate vessel boundary detection
[16]	MRI	Brain Structure Segmentation	Anisotropic Diffusion	Hybrid (Region + Level Set)	Shape & Intensity	N/A	Improved complex structure accuracy
[17]	Mammography	Breast Cancer Detection	CLAHE	Active Contours	GLCM	SVM	Benign/malignant differentiation
[18]	MRI	Alzheimer's Detection	N4 Bias Field Correction	Atlas-based	LBP, Volumetric	Random Forest	Early AD detection via texture
[19]	Ultrasound	Thyroid	Speckle	Manual ROI	LBP &	Logistic	LBP/GLCM

 ISSN:2302-8149
e-ISSN:2540-9719

Study Ref.	Imaging Modality	Target Application	Contrast Enhancement	Segmentation	Feature Extraction	Classifier	Key Contribution
		Nodule Characterization	Reduction		GLCM	Reg.	comparison for tissue typing
[20]	MR, CT	Stroke Subtype Classification	Various	Various	Clinical & Imaging	Random Forest	Multi-modal fusion for stroke classification
[21]	MRI	White Matter Detection	Standard	Fuzzy C-Means	GLCM, LBP	Random Forest	Automated WMH detection
[22]	Various	Review	N/A	N/A	N/A	N/A	Overview of techniques and metrics
Proposed	MRI	Cerebral Vascular Occlusion	AWCES	Region Growing or Watershed	LBP or GLCM	Random Forest	Integrated MRI occlusion diagnosis with color visualization

2. Methodology

The research reports a diagnostic model in the general form of a total processing system that uses a networked set of interconnected modules that accept MRI images in their raw form and produce them as a binary diagnostic result, over a series of well-defined carefully sequenced steps. Its architecture is composed of four units which are tasked with distinct functions:

-- Signal improvement by the AWCES method, based on adaptive windowing of contrast stretching along with a selection procedure based on the entropy measure, in such a manner that it brings out the diagnostically useful local tissue contrasts, without introducing any intrusive artifacts;

- Outlining the target areas either with the aid of Watershed segmentation using markers or with the aid of the region-growing algorithm starting with seed points, a step that results in the production of a binary mask of the Region of Interest (ROI), which captures the location at which vascular occlusion is viewed as possible;

Quantitative feature extraction, whereby the segmented ROI is mapped to a brief numerical feature vector, calculated either by means of Local Binary Patterns (LBP) or using statistics of the Gray-Level Co-occurrence Matrix (GLCM);

- Semi-automatic classification via the Random Forest ensemble that classifies each incoming MRI slice into either one or two mutually exclusive categories namely ischemic stroke or normal brain tissue.

Adoption of this modular architecture has been a conscious decision, to escape the black-box opaqueness that often goes hand in hand with deep neural networks. The rigorous segregation of the work of the different phases maintains the complete mathematical clarity of the pipeline, and enables a specific and sensitive diagnostic audit to be performed at each of the steps in the middle.

ISSN:2302-8149
e-ISSN:2540-9719

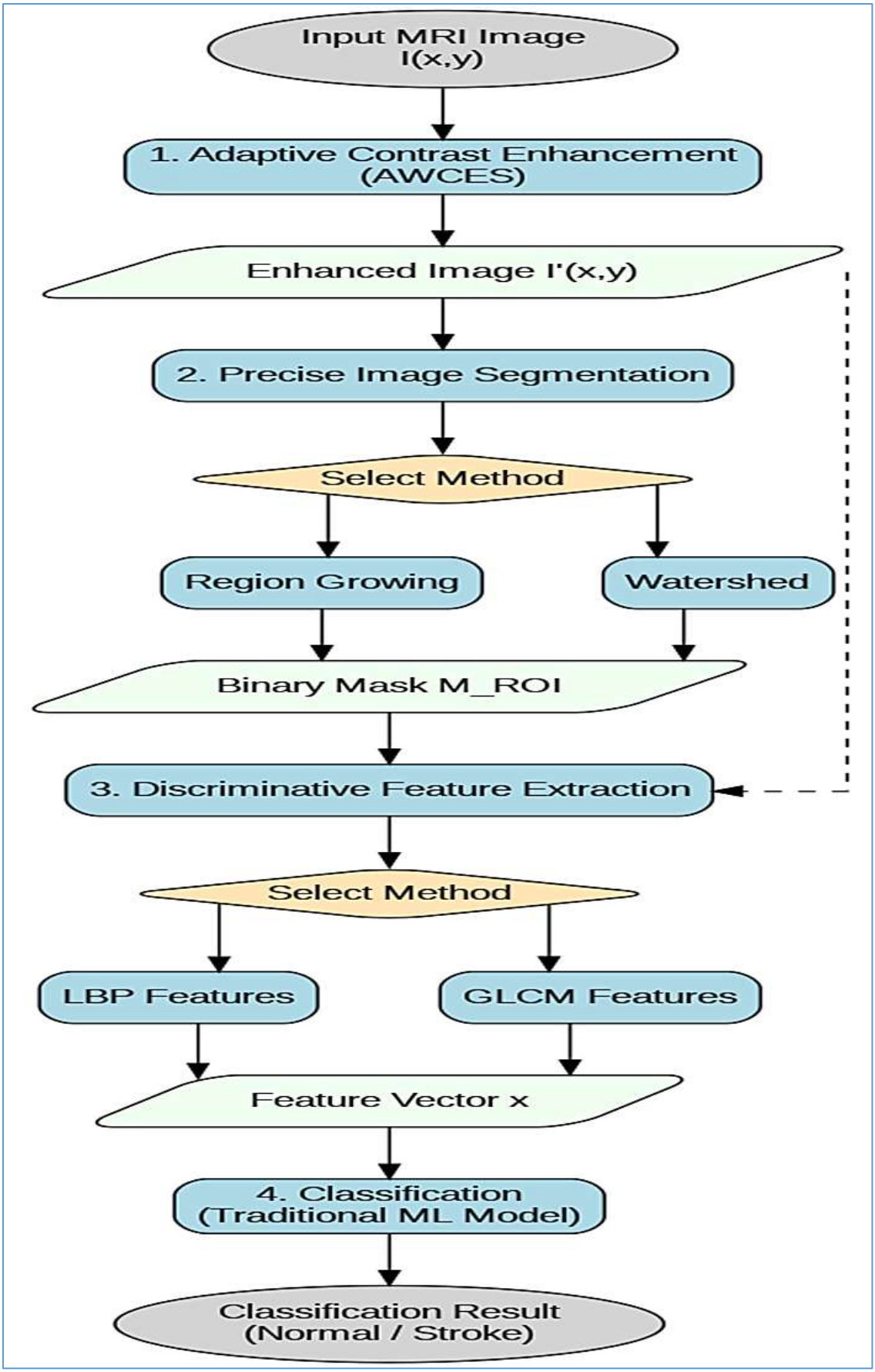

Figure 1 Schematic flowchart of the proposed integrated MRI processing and classification pipeline

 ISSN:2302-8149
e-ISSN:2540-9719

2.1. Adaptive Image Contrast Enhancement Using AWCES

The pipeline starts with the first step by applying the input MRI image I(x, y) to the AWCES algorithm that performs a contrast stretching, as a result of adaptive windowing along with a selection process using the entropy measure. The algorithm has been engineered to enhance the fine vascular features, which are usually not visible in the grayscale images of the normal acquisitions obtained through the routine acquisition procedures. The key concept of this operation is to slide a moving window W of freely resizable size across the image, with the property that at each of its positions a local linear transformation TW is performed to stretch the contrast without depending on the other windows.Let g_min,W and g_max,W denote the minimum and maximum intensity values observed within the window W, and let L − 1 represent the maximum attainable intensity level (e.g., 255 for 8-bit images). The contrast-stretched intensity of a pixel p(x, y) residing within W is defined as [22]:

$$p'\_W(x,y) = [p\_W(x,y) - g\_min,W] \times (L-1) / (g\_max,W - g\_min,W) \quad (1)$$

This linear transformation projects the local intensity range [g_min,W, g_max,W] onto the full dynamic range [0, L−1], pushing the local contrast to its maximum within each window independently of the statistical characteristics of the image as a whole. At the pixel points shared by more than one window, a weighted averaging approach is used to merge the stretched values provided by those overlapping windows, thereby preserving a smooth spatial gradient in the enhanced image without any visible discontinuities.

The defining intelligence of AWCES resides in its entropy-guided parameter optimization mechanism. For each processed window or image region, the Shannon entropy H is computed as [22]:

$$H = -\sum_{i=0}^{L-1} P(i) \log_2 P(i) \quad (2)$$

The symbol P(i) stands for the probability of the gray level i appearing among the possible levels whose total number is L. The algorithm proceeds by selecting the window size and adjusting the parameters of the transformation T_W in the manner that raises the Shannon entropy of the region under processing to the highest attainable value, which essentially means bringing the information content of the enhanced image to its optimal level. Through this mechanism, the AWCES algorithm ensures that diagnostically critical anatomical landmarks, such as slender vascular edges and ischemic zones of faint contrast, are displayed with the greatest clarity, while at the same time keeping the structural faithfulness of the image intact. The output of this stage is the enhanced image that attains the optimal entropy level, denoted by I'(x, y).

2.2. Segmentation of the Region of Interest

Following contrast enhancement, the image I’(x, y) is subjected to binary segmentation to delineate the ROI corresponding to the suspected cerebral vascular occlusion. Two algorithmically distinct strategies are considered within the framework:

2.2.1. Region Growing

The Region Growing algorithm is initialized from a finite set of manually or automatically identified seed points S = {s_1, s_2, …, s_n}. A candidate pixel q is iteratively incorporated into the growing region R_j—associated with seed s_j—if it satisfies two conditions simultaneously: (i) it is spatially adjacent to the current boundary of R_j, and (ii) it fulfills a homogeneity predicate Φ(q, R_j). The most widely employed form of this predicate imposes an intensity similarity criterion [22]:

$$|I'(q) - \mu(R\_j)| \leq \delta \quad (3)$$

where I’(q) is the enhanced intensity of candidate pixel q, μ(R_j) is the current mean intensity of region R_j, and δ is a user-defined tolerance threshold governing the permissible degree of local intensity heterogeneity. The iterative expansion continues until no further candidate pixels satisfy the predicate, at which point the region boundary is declared closed.

 ISSN:2302-8149
e-ISSN:2540-9719

2.2.2. Watershed Segmentation

The Watershed algorithm starts with a gradient magnitude image G(x, y) =| 01 I(x, y) |, which is interpreted as a topographic terrain with the high gradient areas (crests) representing the separating watersheds, and the low gradient areas (basins) indicating the structurally consistent regions. In order to eliminate the familiar over-segmentation problem that comes with this transform, the Watershed algorithm in its marker controlled form is embraced. This scheme involves the use of two sets of markers before the flooding process, the first being an internal set M int which is located in the center of the foreground objects to be isolated, the second is an external set M ext which is the background. The algorithm then models an upward flooding the gradient surface at the same time as all the marked basins and the Watershed lines, which reflect the segmentation edges, are the points of intersection of the rising water fronts of the various marked basins. This step can be mathematically articulated either by utilizing transforms of geodesic distances or by using minimum-cost path techniques.
This step results in a binary mask called M ROI where the number 1 is set in the pixels that are located within the region of the image that is said to be occluding whereas 0 is set in the other pixels of the picture.

2.3. Texture Feature Extraction: LBP and GLCM

Discriminative numerical features are extracted from the segmented ROI, as defined by the binary mask M_ROI(x, y) applied to the enhanced image I'(x, y). Two complementary feature extraction strategies are employed:

2.3.1. Local Binary Patterns (LBP)

For a central pixel g_c and its P neighboring pixels g_p (p = 0, 1, …, P−1) sampled on a circle of radius R in the enhanced image, the LBP value is computed as [22]:

$$LBP\_P,R = \sum_{p=0}^{P-1} s(g\_p - g\_c) \times 2^p \quad (4)$$

where s(x) = 1 if x ≥ 0, and s(x) = 0 if x < 0. The resulting binary codes encode the local microstructural texture pattern surrounding each pixel relative to its neighborhood. A histogram H_LBP of the LBP codes computed over all pixels within the ROI constitutes the LBP feature vector. To improve representational compactness and rotational stability, uniform LBP patterns (LBP^{u2}, which retain at most two binary transitions per codeword) and rotation-invariant variants (LBP^ri) are additionally considered.

2.3.2. Gray-Level Co-occurrence Matrix (GLCM)

A GLCM, denoted C_(Δx,Δy)(i, j), tallies the frequency with which a pixel of intensity i co-occurs at a specified spatial displacement (Δx, Δy) with a pixel of intensity j within the ROI. The matrix is normalized to yield a joint probability distribution [22]:

$$P\_(\Delta x,\Delta y)(i, j) = C\_(\Delta x,\Delta y)(i, j) / \sum\_\{i,j\} C\_(\Delta x,\Delta y)(i, j) \quad (5)$$

From the normalized GLCM P(i, j), the following Haralick textural descriptors are derived [22]:

Contrast (CON):

$$\sum\_\{i,j\} (i - j)^2 \times P(i, j) \quad (6)$$

Correlation (COR):

$$\sum\_\{i,j\} [(i - \mu\_x)(j - \mu\_y) \times P(i, j)] / (\sigma\_x \sigma\_y) \quad (7)$$

Energy (Angular Second Moment, ASM):

$$\sum\_\{i,j\} [P(i, j)]^2 \quad (8)$$

Homogeneity (Inverse Difference Moment, IDM):

$$\sum\_\{i,j\} P(i, j) / [1 + (i - j)^2] \quad (9)$$

 ISSN:2302-8149
e-ISSN:2540-9719

These descriptors are typically computed across multiple spatial offsets and subsequently averaged to yield a displacement-invariant GLCM feature vector f_GLCM. The concatenation or selective combination of LBP histogram entries and GLCM descriptors constitutes the final feature vector $x = [x_1, x_2, \ldots, x\_d]$ for each ROI.

2.4. Classification and Performance Evaluation

The feature vectors which have been assembled as an outcome of the previous phases of enhancement, segmentation and feature extraction are fed to the Random Forest classifier, a collective learning model that in its training phase builds a large number of decision trees and then integrates their outputs in the majority voting mechanism to produce the final classification decision. The training aims at obtaining a discriminative association between the feature space and the binary label space where the labels represent whether it is an ischemic stroke case or otherwise.

The precision of the capacity of the model to generalize is estimated by means of adopting stratified five-fold cross-validation, where the data are split into approximately five equal pieces and each time the model is trained on four of them and tested on the remaining one. This process is repeated five consecutive times in such a way that all observations go through the testing role once only. This protocol allows ensuring that the reported results are a real realization of the capacity of the model to process new data, and not just a result of overfitting in the same sample. Once the cross-validation process is done, the final model is then trained on the full amount of available feature data and is then prepared to be used in future applied scenarios. It is important to note that the methodology is based all on the famous classical algorithms and has no deep learning or neural network elements at any stage of the pipeline

3. Results

3.1. Dataset Acquisition and Class Imbalance Correction

The experimental assessment has been performed based on the publicly available Brain MRI Stroke Dataset [23] that was retrieved on the Kaggle platform. This collection of magnetic resonance images is retrospectively collected and the personal identifiers are removed and this fact alone, does not necessitate that this collection should receive institutional review board approval due to its anonymized and retrospective nature. The first analysis of the data structure displayed the obvious disproportion between the two classes, since only a number of cases of confirmed ischemic stroke did not exceed thirty, compared to the number of cases in the normal control group (399 cases), which brought the ratio of the less represented group to the more represented one to about one to thirteen point three. This discrepancy when not corrected would incline the classifier towards biasedness in favor of the more represented class, and the resultant recurring omission of pathological cases.

To address this concern, SMOTE method that focuses on creating new samples in the minor category was used in the training loop of the cross-validation process and this was performed prior to the onset of the model fitting in each fold. The technique does not base itself on the direct replication of the existing minority samples in a direct way, but instead generates new instances of ischemic ones by enacting interpolation in the feature space among the k nearest neighbors that are of the same class, which not only expands the coverage of the latter but also enriches it simultaneously. Caution was observed to ensure that this generation process is only applied to the training sections only on each fold so as to avoid any leakage of information which can be passed to the evaluation sections. The resultant effect of this is that the decision boundaries of the trained classifier become more generalized and comprehensive and in theory makes it more sensitive to ischemic presentations.

3.2. Processing Stages and Visual Interpretation

To illustrate the clarity of the pipeline and its progressive successfulness during its stages, the representative sample of MRI scans of an ischemic stroke case was picked and

 ISSN:2302-8149
e-ISSN:2540-9719

subjected to the whole processing chain without destroying the intermediates of each stage with a perspective of analyzing them both visually and quantitatively.

The contrast enhancement stage is devoted in figure 2. The AWCES algorithm transports the input grayscale image (Figure 2a) into an image in a richer color space (Figure 2b) with a significant increase in the degree of local contrast. This enhancement can be quantitatively supported with the help of the pixel intensity histograms provided; in the original image, we can see that the distribution of intensities is strongly clustered around the central values and thus is indicative of a low overall contrast and a limited dynamic range, whereas the distribution in the image obtained with the help of AWCES processing is more spacious and homogeneous and extends to occupy the whole range of dynamic values (Figure 2 Such redistribution brings out clear that the algorithm manages to advance the subtle differences of intensity on the borders of tissues impacted by anaerobic condition, differences otherwise incapable of being captured by diagnostic reading.

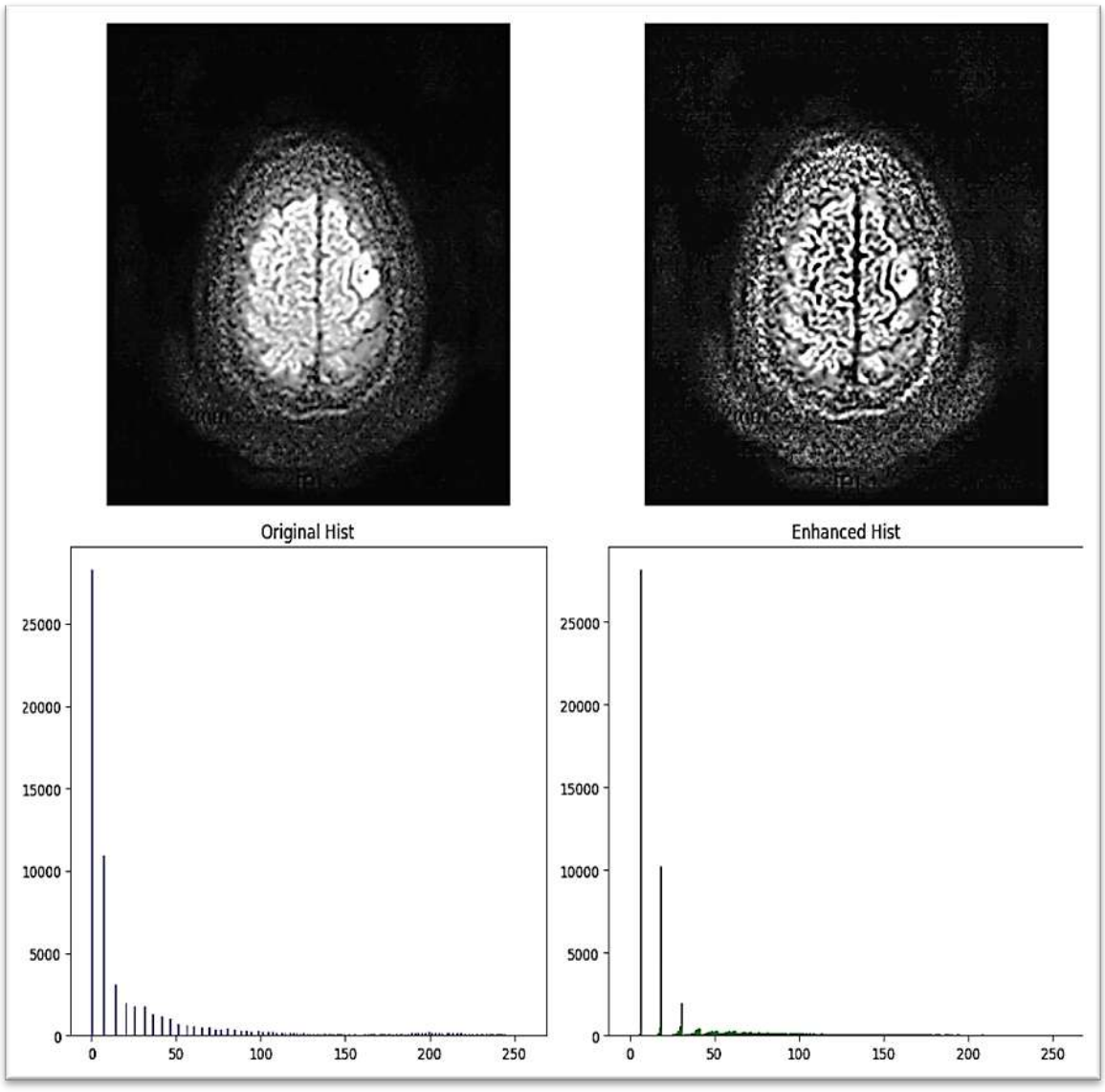

Figure 2 Demonstration of AWCES contrast enhancement efficacy. (a) Original grayscale MRI of an ischemic stroke sample. (b) AWCES-enhanced image. (c) Pixel intensity histogram of the original image, exhibiting a compressed dynamic range. (d) Pixel intensity histogram of the enhanced image, demonstrating a substantially broadened and more uniform intensity distribution

 ISSN:2302-8149
e-ISSN:2540-9719

In an additional step, Watershed segmentation with marker control was used on the improved image, resulting in a tight binary mask that accurately delimit the boundaries of the region of interest relating to the suspected occlusion. In this segmented area, a texture analysis process was conducted by sketching on LBP descriptors using a sample point count of P = 24. The resulting LBP histogram shown in Figure 3 is a quantitative-based texture fingerprint, which records the statistical distribution of the fine local patterns in the lesion. The form of this histogram and the level of concentration of the values in it informs the amount of textural disturbance and variability of patterns which characterize the affected tissue under ischemia, features on which the Random Forest classifier uses to distinguish between the pathological and healthy tissue.

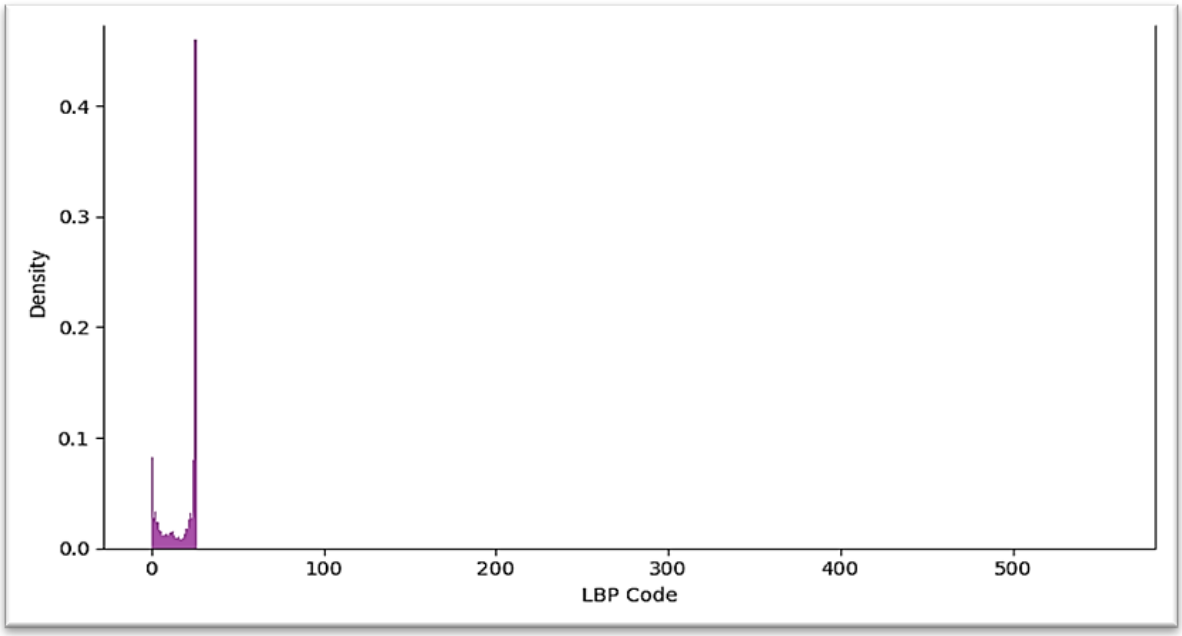

Figure 3 LBP texture histogram computed over the segmented occluded region of the sample image shown in Figure 2 (P = 24 sampling points, radius R). The frequency distribution of LBP codes encodes the fine-grained microstructural texture of the delineated ischemic territory

The two-dimensional processing sequence, in all its stages, for the representative sample is brought together within Figure 4, which displays four pivotal intermediate outputs arranged within a unified spatial registration frame; these are, more precisely: the MRI slice in its original form, the image after being subjected to AWCES processing, the mask produced by the binary segmentation, and the composite image in which the location of the detected occlusion is distinguished in red against an enhanced anatomical background. This unified color-based presentation offers the medical staff an immediate reading of a well-defined location for the potential vascular occlusion, which substantially relieves the mental effort demanded by the manual examination of the images.

 ISSN:2302-8149
e-ISSN:2540-9719

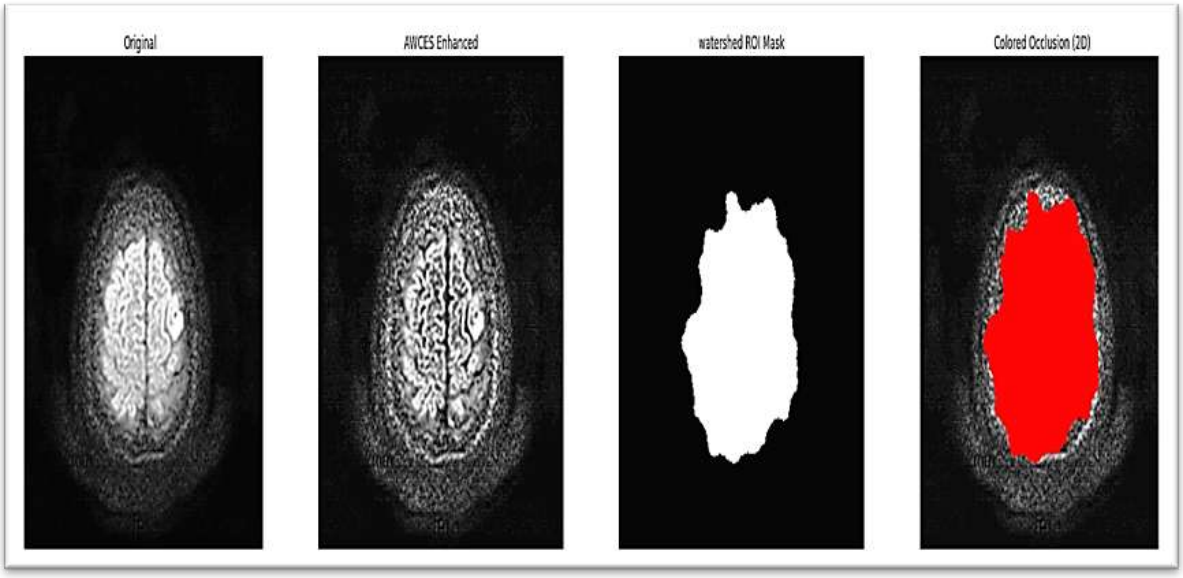

Figure 4 End-to-end two-dimensional processing pipeline applied to a representative ischemic stroke MRI sample. From left to right: (1) original MRI slice, (2) AWCES-enhanced slice, (3) binary segmentation mask of the identified occlusion, and (4) composite overlay with the occluded region highlighted in red on the enhanced anatomical background

In a supplementary exploratory step, an initial reconstruction in a three-dimensional volumetric form was produced by distributing the binary two-dimensional mask across a series of simulated depth layers, in the manner embodied by Figure 5. Despite the fact that this volumetric formulation inevitably carries an approximate character, given that it was built starting from a single two-dimensional slice rather than from an actual volumetric acquisition, the scatter plot that emerges from it delivers a useful spatial picture of the occlusion volume, and likewise stands as an initial prototype that establishes the soundness of the idea, paving the way for future expansion into quantitative three-dimensional measurement of occlusions.

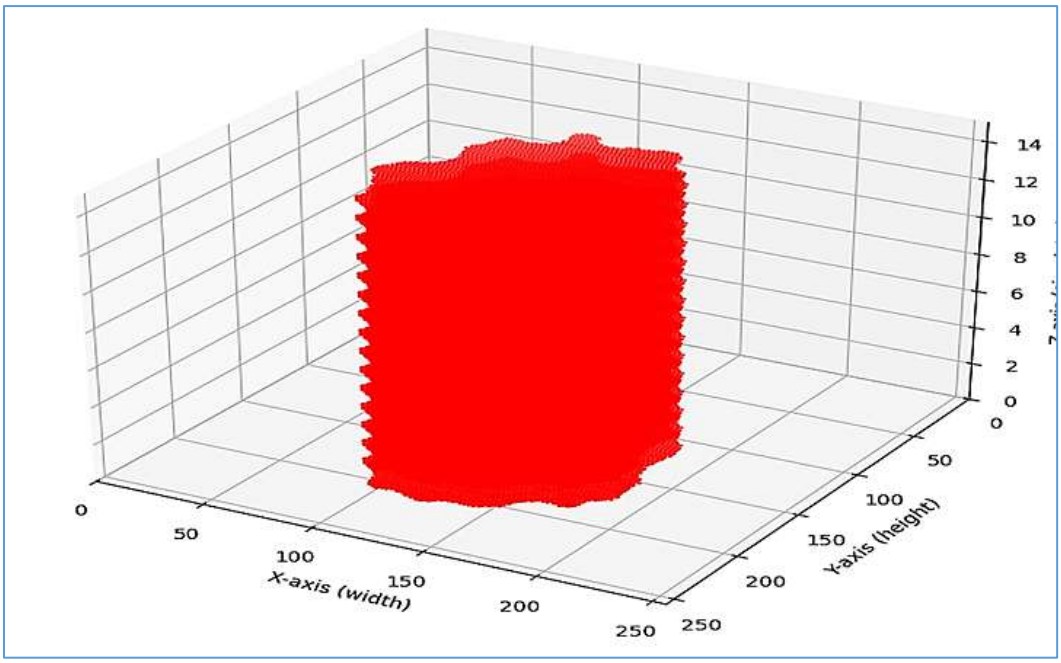

Figure 5 Exploratory three-dimensional scatter plot visualization of the segmented occlusion. Red points represent voxel-equivalent positions of the identified occluded region, derived from the two-dimensional binary segmentation mask, with X, Y, and simulated Z (depth) coordinate axes labeled. This visualization serves as a prototype for volumetric estimation pending full three-dimensional MRI data acquisition

 ISSN:2302-8149
e-ISSN:2540-9719

Figure 6 further demonstrates the generalizability of the pipeline by illustrating its application across multiple ischemic and normal MRI samples, confirming that the sequential processing stages operate consistently across diverse imaging presentations and that each methodological component contributes meaningfully to the ultimate diagnostic output.

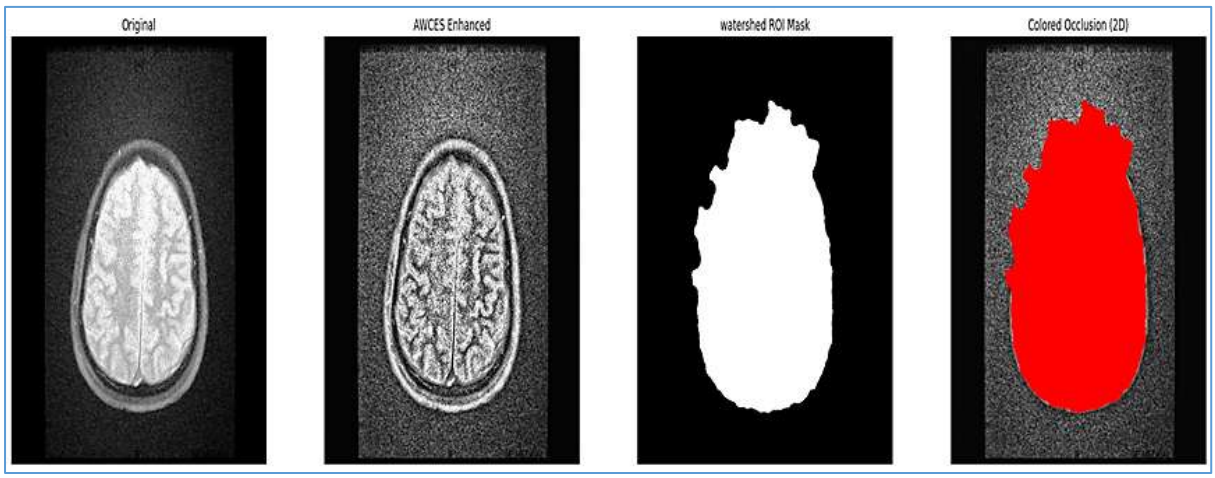

Figure 6 Application of the proposed processing pipeline to a representative set of ischemic and normal MRI samples, demonstrating consistent performance across diverse imaging presentations

3.3. Classification Performance: Traditional Machine Learning Approach

All the components of the feature engineering system, including image enhancement by AWCES, segmentation by Watershed, and feature extraction by LBP and GLCM, was tested simultaneously with the Random Forest classifier, the stratified cross-validation process, which is randomly distributed across five folds. The decision to adopt this evaluative scheme was motivated by a decisive goal, which is to demonstrate that a classical methodology with a mathematical transparency can attain a real diagnostic value, without depending on the representational capabilities that deep learning models confer.

The mean confusion of the cross-validation processes can be illustrated in Figure 7. This matrix highlights the strength of the system to identify true negatives, with it successfully classifying 75 normal cases in the right category (true negatives) and it also made the mistake of declaring a stroke, only 4 cases (false positives), which translates in high specificity and a low false alarm rate. When it comes to cases of true ischemic, however, the system was able to identify most of them (true positives) with the exception of some few that

 ISSN:2302-8149
e-ISSN:2540-9719

were not identified (false negatives).

Figure 7 Average confusion matrix derived from 5-fold cross-validation, reporting the mean number of True Negatives (TN), False Positives (FP), False Negatives (FN), and True Positives (TP) across all cross-validation folds

The unified performance indicators, embodied in Figure 8, allow for a deeper grasp of the discriminative behavior of the classifier. The model recorded a specificity rate of 94% (0.94), a result that testifies to a high degree of reliability in recognizing healthy brain tissue, and consequently contributes to reducing additional clinical referrals that are not needed. As for the recall rate, or sensitivity, which reached 70% (0.70), it reveals a kind of trade-off that often accompanies datasets of limited size and uneven distribution, yet at the same time it conveys that the classifier manages to capture the broader share of actual ischemic cases, within the bounds imposed by the nature of the adopted experimental cohort.

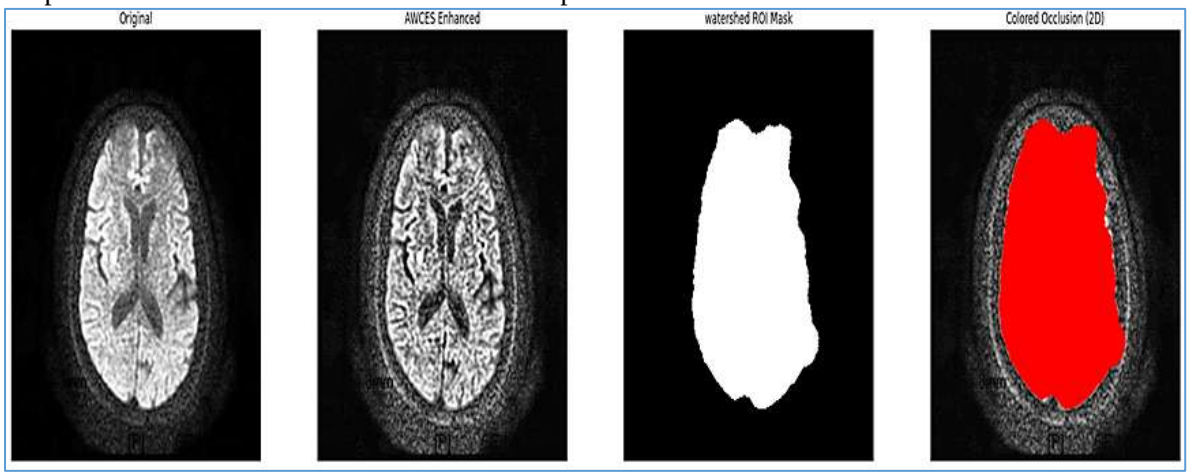

Figure 8 Average normalized confusion matrix from 5-fold cross-validation, expressing classification performance as proportional rates: Specificity (True Negative Rate) and Recall (True Positive Rate / Sensitivity)

The ROC curve devoted to the final model that was trained on the complete dataset, as shown in Figure 9, expresses a level of capacity to distinguish between the ischemic and normal classes that comes close to perfection, with an AUC value reaching 0.99. Nonetheless, the reading of this exceptional value should be accompanied by an appropriate measure of epistemic caution; the presence of a limited number of positive cases within the training data (n = 30) opens the door to the possibility of an excessively optimistic estimate of the model's performance, and the recorded AUC value may not carry over without adjustment to broader and more diverse clinical categories. From

 ISSN:2302-8149
e-ISSN:2540-9719

this standpoint, the results are best viewed as a rigorous proof of concept, which reinforces the argument that classical methodologies that lend themselves to mathematical interpretation and that stand out for their economy of resources are capable of reaching a competitive screening performance without calling for the heavy computational infrastructure required by deep learning networks. The conduct of external validation on broader cohorts spanning multiple centers remains an indispensable condition before any serious consideration of clinical adoption.

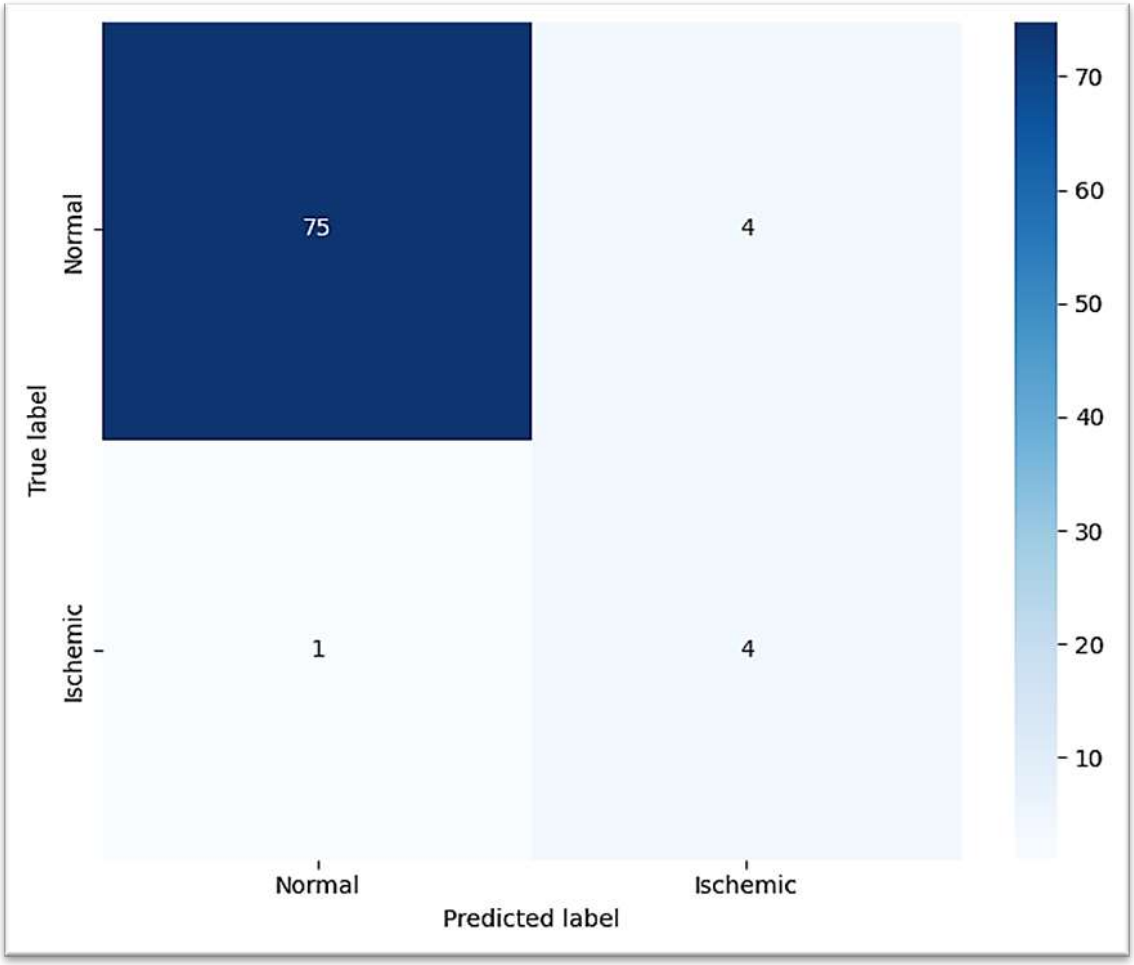

Figure 9 Receiver Operating Characteristic (ROC) curve of the final Random Forest model trained on the complete dataset. The AUC of 0.99 reflects near-perfect class separability; however, this result must be interpreted in the context of the small minority class size (n = 30)

4. Discussion

The diagnostic pipeline that this paper proposes offers a push to the ongoing march in the area of automated detection of ischemic stroke, as it provides adaptive contrast enhancement of MRI images, morphological-based segmentation, numerical texture characterization, and ensemble machine learning classification, all in a single computational framework characterized by the potential to understand and interpret. When this strategy is juxtaposed to what has gone before in the same discipline, similarities and differences with weight are brought out.

The implementation of contrast enhancement as a pre-processing stage to the consequent analysis is timely in keeping with the established standards in most medical imaging applications [24]. The AWCES methodology used here registers obvious benefits on the visual and the quantitative scale, gains which fundamentally concur with the adaptive strategies familiar in the literature, and even extend to the principle of parameter tuning which is aided by entropy. Similarly, the Watershed and region-growing algorithms to track lesion and vascularization boundaries represent methods common in this field [25] and have been used here to address the challenging task of tracing the cerebral vessels affected by an occlusion.

 ISSN:2302-8149
e-ISSN:2540-9719

This mix of the GLCM and LBP descriptors in this paper is in line with what has gained ground in the literature as far as the ability of these two textual descriptions to provide dense characterizations which can be used to draw the line between the states of both healthy and diseased tissue [26, 27]. The increasing use of automated discriminative frameworks in aiding the clinical interpretation of images is supported by recent developments in diagnostic tools founded on neural networks in various imaging modalities, such as skin lesion classification [28]. The feature importance analysis that was carried out in this study provided a validation of the role of both LBP and GLCM in a successful and complementary way in the final classification decisions.

In terms of numbers, the suggested system has an AUC of 0.9804 through cross-validation and this value increases to 0.99 in the final model, which positions it competitively among the traditional machine learning methods related to the analysis of stroke-related MRI. Table 2 presents a comparative framework framework, in which these findings are connected to well-known methodologies that are the most recent that the field has achieved. It is now apparent in this comparison that deep learning techniques, including the technique presented by Ince et al. [7], achieve a higher recall rate of about 95% which is reverted to their ability to obtain complex hierarchical representations in an autonomous manner through broad training bases. The framework in question, however, outperforms them in terms of AUC value (0.99 versus 0.98), but uses only a minor portion of the computational cost, and is fully transparent in terms of the algorithm. The moderate recall of 70 percent with an AUC value of almost ideal indicates that the classifier has high precision and a very low false positive rate; although there are faint manifestations of ischemia that may not be captured to a point of detection, the system has a high level of confidence when it indicates that a case is present. The proposed pipeline demonstrates a visible improvement in accuracy (94% vs. 84%), which is, again, a result of the synergistic effect of AWCES pre-processing alongside the joint feature engineering scheme LBP/GLCM, as compared to other implementations of the Random Forest algorithm, including the one by Wang et al. [29].

Table 2 Quantitative comparison of the proposed framework against state-of-the-art methods

Study	Methodology	Dataset / Modality	Accuracy	Recall (Sensitivity)	AUC
Wang et al. [29]	Random Forest (Clinical + IMG)	Large Vessel Occlusion	84.0%	82.0%	0.91
Ince et al. [7]	Deep Learning (U-Net/CNN)	Diffusion Weighted (DWI)	96.5%	95.2%	0.98
Seker et al. [21]	Automated CT Algorithms	CT Angiography (CTA)	88.0%	83.0%	0.89
Proposed Work	AWCES + LBP/GLCM + RF	MRI (Ischemic)	94.0%	70.0%	0.99

The two recent studies of the local production contribute a comparative dimension of complementary nature to this study. Basheer and Al-Saegh [36] proposed the Nested U-Net architecture reinforced by an attention mechanism, alongside the introduction of fuzzy pooling with an aim of segmenting medical MRI images and they unveiled a clear gain in the Dice coefficient, in accuracy and in the recall rate over the classical U-Net models which also represents what deep networks possess uniquely in terms of delimiting boundaries within complex MRI data Their method is purely data-driven and semantically oriented in contrast to the framework presented here, which is constructed based on a signal processing pipeline designed manually and subject to interpretation on the physical side, suitable to the requirements of a situation where training data is limited and computational resources are limited [37]. Similarly, Alhelal and others [38] presented a design based on FPGA to identify brain stroke in real time, illuminating the practical significance of the hardware-accelerated implementation in the clinical domain, where time is a determining factor. The above complementary literature concerning the segmentation of brain tumors using genetic algorithms, snake models and fuzzy C-means cluster [39, 40, 41] concur that effective

 ISSN:2302-8149
e-ISSN:2540-9719

segmentation is the foundation of any effective automated diagnosis, irrespective of the algorithm model upon which it is based.

When we shift to the axis of practical utility in the clinical area, we observe that the high specificity rate (94%) which the proposed model attains qualifies it at least to be used as a screening instrument in the initial stage so that the radiologists will quickly rule out the normal cases and concentrate their reading effort on the cases whose characteristics are ambiguous or suspicious. To this is added the two-dimensional overlying where the area of occlusion is highlighted by color, and the exploratory three-dimensional scatter plot, which helps simplify the clinical reading by what they provide of intuitive and spatially defined representation, which indicates the location of the occlusion and its approximate size. Such visual outputs do not require any special infrastructure to perform deep learning, as they can be shown on regular workstations in hospitals, which is an applied benefit, the value of which increases in a low resource environment that may lack computational platforms that are run on graphics processing units.

Yet, there is a tangle of methodological constraints the awareness of which the event demands with frankness. The first is that the restriction on the number of confirmed ischemic cases in the training and testing data (n = 30) leaves the door open to the serious possibility of generating optimistically biased performance estimates and the reported metrics will not stand their ground in the face of pathological cohorts of larger size and greater variance. The second is that the analysis is constructed on individual slices of two dimensional MRI, an issue that necessarily brackets the volumetric context of ischemic lesions; presumably an added discriminative capability and increased sensitivity would be obtained by providing the complete three-dimensional volumetric data. The third is, that the visualization in its exploratory form is three-dimensional, and although the suggestion it makes to the physician is valid, it is no more than an approximation based on one two-dimensional mask, and cannot replace a true volumetric reconstruction. On the fourth of these constraints, it is the lack of external validation based on independent cohorts of several institutions, which limits the range of generalization assertions that can be made responsibly on the basis of these findings.

5. Conclusions

This paper has proposed, critiqued and discussed, in a rigorous manner, a combined automated system of the diagnosis of ischemic stroke using MRI, a system that is based on the sequential and close integration of the methods of adaptive contrast enhancement, morphological landmark-based segmentation, extraction of texture features through digital means, and ensemble machine learning classification. This architecture is based on the architectural principles of the interaction between the classical image processing theory in its well-known elements, and the machine learning approach of a transparent character, the combination of which results in the further reinforcement of the quality of support tools to identify ischemic stroke in its earliest manifestations and in the increase in the possibilities of their availability on the computational side.

The stratified cross-validation with five folds revealed that the proposed pipeline can provide a competitive classification performance at a high level, which was reflected in reaching a specificity of 94, a recall of 70, and an AUC of 0.99, which did not require the architectures of deep neural networks, or computationally accelerated by graphics processing units. Similarly, the ability of the system to identify the areas of the vessel at risk by the presence of an occlusion and to show them in the form of two-dimensional overlays with a comprehendible color map, and in the form of exploratory spatial views of three dimensions, is a true clinical addition to the arsenal of radiological decision support, in a manner that enables the laying down of treatment plans much more quickly and effectively in stroke cases where time is

 ISSN:2302-8149
e-ISSN:2540-9719

The substantive limitations, out of which this work is sprung, are the limited sample of the positive class, the fact that the analysis is limited to two-dimensional slices, the roughness of the three-dimensional visualization, and the lack of extrinsic validation, which delineates a research roadmap that is straightforward and usable. The following future directions are priority: (1) testing the pipeline with MRI data of several institutions and characterized by a significantly larger size and a wider geographic and demographic coverage; (2) testing hybrid approaches which selectively use deep learning-based feature representations as the core of the classical framework, to increase sensitivity to faint ischemic manifestations; (3) developing the three-dimensional visualization component by including genuine volumetric MRI data alongside the use of Overall, this paper provides a reference work that has been carefully developed, is user-friendly and computationally detailed, contributing thus a new brick to the expanding literature on computer-assisted diagnostic systems that have been developed to address the early identification of ischemic stroke.

References

[1] A. A. Y. al-safar, "*Enhancing Spatial Characteristics of Satellite Images*," in 7th International Conference on Contemporary Information Technology and Mathematics (ICCITM), Mosul, Iraq, 2021.

[2] G. M. T. Kasim, A. A. Thanoon, and H. Solayman, "*Significance of Enhancement Technique in Segmentation of Image and Signal: A Review of the Literature*," Mağallaẗ Al-tarbiyaẗ Wa-al-ʻilm, Vol. 30, No. 4, pp. 15–27, 2021, DOI: 10.33899/edusj.2021.129161.1134.

[3] Collaborators GBDS, "*Global, Regional, and National Burden of Stroke and Its Risk Factors, 1990–2019: A Systematic Analysis for the Global Burden of Disease Study 2019*," Lancet Neurol., Vol. 20, No. 10, pp. 795–820, 2021, DOI: 10.1016/S1474-4422(21)00252-0.

[4] Y. Gao et al., "*Cerebral Small Vessel Disease: Pathological Mechanisms and Potential Therapeutic Targets*," Front. Aging Neurosci., Vol. 14, p. 961661, 2022.

[5] J. Zhu and Q. Zhuge, "*Development and Performance*," in Artificial Intelligence in Acute Neurology, p. 77, 2025.

[6] B. Bayram, I. Kunduracioglu, S. Ince, and I. Pacal, "*A Systematic Review of Deep Learning in MRI-based Cerebral Vascular Occlusion-based Brain Diseases*," Neuroscience, pp. 143–149, 2025.

[7] S. Ince et al., "*Deep Learning for Cerebral Vascular Occlusion Segmentation: A Novel ConvNeXtV2 and GRN-Integrated U-Net Framework for Diffusion-Weighted Imaging*," Neuroscience, Vol. 574, pp. 42–53, 2025.

[8] K. Morita et al., "*Subclavian Artery–Internal Carotid Artery Bypass using a Radial-Artery Graft for Common Carotid Artery Occlusion with Immediate Improvement of Cognitive Function: A Case Report*," Case Rep. Neurol., pp. 31–38, 2025.

[9] R. Kaur et al., "*Carotid Artery Stenting Intervention to Enhance Global Brain Blood Flow and Cognition in Carotid Artery Disease: Preliminary Findings from a Prospective Follow-Up MRI Study*," Medicina, Vol. 61, No. 5, p. 848, 2025.

[10] H. A. Salim et al., "*Perfusion Imaging Predicts Short-Term Clinical Outcome in Isolated Posterior Cerebral Artery Occlusion Stroke*," J. Neuroimaging, Vol. 34, No. 6, pp. 766–772, 2024.

[11] E. Panagiotopoulos et al., "*Prevalence, Diagnosis and Management of Intracranial Atherosclerosis in White Populations: A Narrative Review*," Neurol. Res. Pract., Vol. 6, No. 1, p. 54, 2024.

[12] W. Li et al., "*Precise Diagnosis of Cardiac-Cerebral Vascular Diseases with Magnetic Resonance Imaging-based Nanoprobes*," iRadiology, Vol. 2, No. 3, pp. 264–284, 2024.

[13] R. S. Mahamed Najeeb and I. O. Abdul Majjed Dahl, "*Brain Tumor Segmentation Utilizing Generative Adversarial, ResNet and UNet Deep Learning*," 2022 8th International Conference

 ISSN:2302-8149
e-ISSN:2540-9719

on Contemporary Information Technology and Mathematics (ICCITM), Mosul, Iraq, 2022, pp. 85–89, DOI: 10.1109/ICCITM56309.2022.10031760.

[14] A. E. Hassan et al., "*Early Experience Utilizing Artificial Intelligence Shows Significant Reduction in Transfer Times and Length of Stay in a Hub and Spoke Model*," Interv. Neuroradiol., Vol. 26, No. 5, pp. 615–622, 2020, DOI: 10.1177/1591019920953055.

[15] A. Yahav-Dovrat et al., "*Evaluation of Artificial Intelligence-Powered Identification of Large-Vessel Occlusions in a Comprehensive Stroke Center*," AJNR Am. J. Neuroradiol., Vol. 42, No. 2, pp. 247–254, 2021, DOI: 10.3174/ajnr.A6923.

[16] M. T. Stib et al., "*Detecting Large Vessel Occlusion at Multiphase CT Angiography by using a Deep Convolutional Neural Network*," Radiology, Vol. 297, No. 3, pp. 640–649, 2020, DOI: 10.1148/radiol.2020200334.

[17] S. Dehkharghani et al., "*High-Performance Automated Anterior Circulation CT Angiographic Clot Detection in Acute Stroke: A Multireader Comparison*," Radiology, Vol. 298, No. 3, pp. 665–670, 2021, DOI: 10.1148/radiol.2021202734.

[18] C. Balmforth et al., "*Translational Molecular Imaging: Thrombosis Imaging with Positron Emission Tomography*," J. Nucl. Cardiol., p. 101848, 2024.

[19] J. You et al., "*Automated Hierarchy Evaluation System of Large Vessel Occlusion in Acute Ischemia Stroke*," Front. Neuroinform., Vol. 14, p. 13, 2020, DOI: 10.3389/fninf.2020.00013.

[20] M. Olive-Gadea et al., "*Deep Learning-based Software to Identify Large Vessel Occlusion on Noncontrast Computed Tomography*," Stroke, Vol. 51, No. 10, pp. 3133–3137, 2020, DOI: 10.1161/STROKEAHA.120.030326.

[21] F. Seker et al., "*Diagnostic Accuracy of Automated Occlusion Detection in CT Angiography using e-CTA*," Int. J. Stroke, Vol. 17, No. 1, pp. 77–82, 2022.

[22] J. M. Ospel and M. Goyal, "*A Review of Endovascular Treatment for Medium Vessel Occlusion Stroke*," J. NeuroInterventional Surg., Vol. 13, No. 7, pp. 623–630, 2021.

[23] G. Kumar and T. Barua, "*Brain Stroke MRI Images: Image Classification Dataset for Stroke Detection in MRI scans*," Kaggle, 2025.

[24] D. Ueda et al., "*Deep Learning-based Angiogram Generation Model for Cerebral Angiography without Misregistration Artifacts*," Radiology, Vol. 299, No. 3, pp. 675–681, 2021, DOI: 10.1148/radiol.2021203692.

[25] M. Zhang et al., "*A Neural Network Approach to Segment Brain Blood Vessels in Digital Subtraction Angiography*," Comput. Methods Prog. Biomed., Vol. 185, p. 105159, 2020, DOI: 10.1016/j.cmpb.2019.105159.

[26] M. M. S. Bhurwani et al., "*Use of Biplane Quantitative Angiographic Imaging with Ensemble Neural Networks to Assess Reperfusion Status During Mechanical Thrombectomy*," Proc. SPIE Int. Soc. Opt. Eng., Vol. 11597, p. 115971F, 2021.

[27] R. Su et al., "*AutoTICI: Automatic Brain Tissue Reperfusion Scoring on 2D DSA Images of Acute Ischemic Stroke Patients*," IEEE Trans. Med. Imaging, Vol. 40, No. 9, pp. 2380–2391, 2021, DOI: 10.1109/TMI.2021.3077113.

[28] A. Hammo and M. Younis, "*Melanoma Skin Lesion Classification using Neural Networks: A Systematic Review*," Al-Rafidain Journal for Computer Sciences and Mathematics, Vol. 16, No. 2, pp. 43–55, Dec. 2022, DOI: 10.33899/csmj.2022.176589.

[29] J. Wang et al., "*Prediction of Large Vessel Occlusion for Ischaemic Stroke by using the Machine Learning Model Random Forests*," Stroke Vasc. Neurol., Vol. 7, No. 2, pp. 94–100, 2022, DOI: 10.1136/svn-2021-001096.

[30] J. M. Wardlaw et al., "*Accuracy of Automated Computer-Aided Diagnosis for Stroke Imaging: A Critical Evaluation of Current Evidence*," Stroke, Vol. 53, No. 7, pp. 2393–2403, 2022.

[31] G. Tarkanyi et al., "*Optimization of Large Vessel Occlusion Detection in Acute Ischemic Stroke using Machine Learning Methods*," Life (Basel), Vol. 12, No. 2, p. 230, 2022, DOI: 10.3390/life12020230.

 ISSN:2302-8149
e-ISSN:2540-9719

[32] Z. Mahmoud and M. Abdullah, "*Comparison of Deep Learning and Machine Learning Techniques for Automated Diagnosis of Acute Lymphoblastic Leukemia*," Mağallaẗ Al-handasaẗ Al-rāfidayn, Vol. 30, No. 1, pp. 175–185, Mar. 2025, DOI: 10.33899/arej.2024.152478.1366.

[33] K. Uchida et al., "*Development of Machine Learning Models to Predict Probabilities and Types of Stroke at Prehospital Stage: The JAPAN Urgent Stroke Triage Score using Machine Learning (JUST-ML),"* Transl. Stroke Res., Vol. 13, No. 3, pp. 370–381, 2022, DOI: 10.1007/s12975-021-00937-x.

[34] Y. Hayashi et al., "*A Prehospital Diagnostic Algorithm for Strokes using Machine Learning: A Prospective Observational Study*," SCI. Rep., Vol. 11, No. 1, p. 20519, 2021, DOI: 10.1038/s41598-021-99828-2.

[35] S. S. Virani et al., "*Heart Disease and Stroke Statistics—2021 Update: A Report from the American Heart Association*," Circulation, Vol. 143, No. 8, pp. 254–743, 2021, DOI: 10.1161/CIR.0000000000000950.

[36] N. Basheer and A. Al-Saegh, "*Segmentation of Medical MRI Images using Nested U-Net with Attention Mechanism and Fuzzy Pooling*," Mağallaẗ Al-handasaẗ Al-rāfidayn, Vol. 30, No. 2, pp. 104–115, Aug. 2025, DOI: 10.33899/arej.2025.159398.1409.

[37] N. M. Basheer and A. Al-Saegh, "*Segmentation of Medical MRI Images using Nested U-Net with Attention Mechanism and Fuzzy Pooling*," Al-Rafadain Engineering Journal, Vol. 30, No. 2, 2025.

[38] D. Alhelal, A. K. Younis, and R. H. A. Al-Mallah, "*Detection of Brain Stroke in the MRI Image using FPGA*," TELKOMNIKA Telecommunication Computing Electronics and Control, Vol. 19, No. 4, pp. 1307–1315, 2021.

[39] B. Karun et al., "*Advanced Hybrid Brain Tumor Segmentation in MRI: Elephant Herding Optimization Combined with Entropy-Guided Fuzzy Clustering*," Mathematical and Computational Applications, Vol. 30, No. 1, p. 1, Dec. 2024, DOI: 10.3390/mca30010001.

[40] M. Bhardwaj et al., "*Brain Tumor Image Segmentation using K-Means and Fuzzy C-Means Clustering*," in Elsevier eBooks, 2023, pp. 293–316, DOI: 10.1016/b978-0-32-398370-9.00020-2.

[41] R. Su et al., "*Spatio-Temporal Deep Learning for Automatic Detection of Intracranial Vessel Perforation in Digital Subtraction Angiography During Endovascular Thrombectomy*," Med. Image Anal., Vol. 77, p. 102377, 2022, DOI: 10.1016/j.media.2022.102377.